

Thermochemical Properties, Reaction Paths and Kinetic Mechanism for Sulfur-Chloro Hydrocarbon Combustion: Part I: Thermochemistry and Pyrolysis of Chlorosulfides

Christopher J. Montgomery, Michael J. Bockelie, Adel F. Sarofim
Reaction Engineering International, Salt Lake City, UT 84101

Jongwoo Lee, and Joseph W. Bozzelli
Department of Chemical Engineering, Chemistry, and Environmental Science
New Jersey Institute of Technology, Newark, NJ 07102

Abstract

Almost no data exists in the literature on thermochemical properties— enthalpy of formation, entropy or heat capacities – for chlorinated sulfur hydrocarbons and oxygenated intermediates in atmospheric or thermal oxidation reactions. Even less kinetic data exists on the elementary processes involved in these reaction systems. This study describes a first attempt to generate a thermochemical property data set and an elementary reaction mechanism for pyrolysis and oxidation of diethyl sulfide and dichloro-diethyl sulfide.

Standard enthalpy of formation, $\Delta H_{f,298}^0$, entropy, S_{298}^0 , and heat capacities $C_p(T)$, are determined for stable molecules, intermediates, and transition states in oxidation of sulfur containing hydrocarbons using DFT (Density Functional) calculations with the B3LYP and the KM-LYP functionals. *Ab initio* calculations, using the CBS-Q composite method are also used. Benson-type groups for group additivity estimation of oxygenated sulfur hydrocarbons are constructed.

Enthalpies of formation (ΔH_f°) are determined using the Density Functional and CBSQ methods and working reaction analysis with isodesmic or group balance constraints. Entropy (S) and heat capacity ($C_p(T)$), values from vibrational, translational, and external rotational contributions are calculated using the rigid-rotor-harmonic-oscillator approximation, based on the vibration frequencies and structures obtained from the density functional studies. The contribution to S and $C_p(T)$ from analysis on the internal rotors is incorporated into the analysis instead of the more conventional use of torsion frequencies. This is an important consideration in the thermochemical and kinetic analysis; because of the loss of internal rotors in transition states. The important, (low energy barrier) paths for unimolecular dissociation of the parent sulfur chlorocarbons are HCl elimination, retro-ene, and carbon sulfur bond cleavage reactions. These are however, all above 50 kcal/mol in barrier.

Details on the thermochemistry and kinetic parameters for thermal reactions are presented herein. A detailed pyrolysis and oxidation mechanism is constructed using hydrocarbon and chlorocarbon oxidation using nitrogen–oxygen mechanisms from the literature, and sulfur-hydrocarbon reactions from this study. A detailed chemical kinetic mechanism for HD pyrolysis and oxidation has been created using kinetics and thermodynamic properties generated in this work combined with published sulfur, chlorine, nitrogen, and hydrocarbon kinetics. Sensitivity analysis is used to determine important HD destruction pathways.

Report Documentation Page				Form Approved OMB No. 0704-0188	
Public reporting burden for the collection of information is estimated to average 1 hour per response, including the time for reviewing instructions, searching existing data sources, gathering and maintaining the data needed, and completing and reviewing the collection of information. Send comments regarding this burden estimate or any other aspect of this collection of information, including suggestions for reducing this burden, to Washington Headquarters Services, Directorate for Information Operations and Reports, 1215 Jefferson Davis Highway, Suite 1204, Arlington VA 22202-4302. Respondents should be aware that notwithstanding any other provision of law, no person shall be subject to a penalty for failing to comply with a collection of information if it does not display a currently valid OMB control number.					
1. REPORT DATE OCT 2003		2. REPORT TYPE		3. DATES COVERED 00-00-2003 to 00-00-2003	
4. TITLE AND SUBTITLE Thermochemical Properties, Reaction Paths and Kinetic Mechanism for Sulfur-Chloro Hydrocarbon Combustion: Part I: Thermochemistry and Pyrolysis of Chlorosulfides				5a. CONTRACT NUMBER	
				5b. GRANT NUMBER	
				5c. PROGRAM ELEMENT NUMBER	
6. AUTHOR(S)				5d. PROJECT NUMBER	
				5e. TASK NUMBER	
				5f. WORK UNIT NUMBER	
7. PERFORMING ORGANIZATION NAME(S) AND ADDRESS(ES) Reaction Engineering International ,77 West 200 South Suite 210,Salt Lake City,UT,84101				8. PERFORMING ORGANIZATION REPORT NUMBER	
9. SPONSORING/MONITORING AGENCY NAME(S) AND ADDRESS(ES)				10. SPONSOR/MONITOR'S ACRONYM(S)	
				11. SPONSOR/MONITOR'S REPORT NUMBER(S)	
12. DISTRIBUTION/AVAILABILITY STATEMENT Approved for public release; distribution unlimited					
13. SUPPLEMENTARY NOTES The original document contains color images.					
14. ABSTRACT					
15. SUBJECT TERMS					
16. SECURITY CLASSIFICATION OF:			17. LIMITATION OF ABSTRACT	18. NUMBER OF PAGES 27	19a. NAME OF RESPONSIBLE PERSON
a. REPORT unclassified	b. ABSTRACT unclassified	c. THIS PAGE unclassified			

Introduction

Bis(2-chloroethyl) sulfide, $(\text{ClCH}_2\text{CH}_2)_2\text{S}$ is a main component of the chemical warfare agent HD or mustard gas, as has been recognized since the late 1800's. It has been manufactured in quantity and relatively pure form since the early 1910's. More recently, within the last decade or so, chemical warfare agents are being destroyed due to their potentially harmful effects to civilian populations. The HD (bis(2-chloroethyl) sulfide) is a liquid, that has a relatively low vapor pressure, relative to phosgene ($\text{Cl}_2\text{C}=\text{O}$) or hydrogen cyanide (HCN). The low volatility is due to its' moderately high molecular weight, it boils near 220 C. The high toxicity of HD, similar to that of phosgene and HCN, make experimental studies on this species difficult. In effect, there are very limited studies on it and other agents^{1,2}, and their reliability has been criticized³.

Mustard gas was manufactured in large quantities during World Wars I and II, but has not been manufactured on an industrial basis in the United States since 1968. Stockpiles of mustard gas are stored at seven locations scattered around the United States. Incineration has been selected by the United States as one of the methods for destroying highly toxic chemical agents and munitions contained within the chemical weapons stockpile. As part of the Chemical Stockpile Disposal Program mandated by Congress, the U.S. Army currently uses the baseline incineration system for destruction of munitions and bulk agents containing mustard gas. Incineration technology has been used at two sites, and is under construction/systemization at three additional sites. The scientific and engineering aspects of chemical weapons incineration were reviewed by Gouldin & Fisher⁴. A simulation tool⁵ for analyzing chemical demilitarization incinerators is being developed to help reduce the time, cost and technical risk of destroying the stockpile (Denison). Such a tool requires a detailed model of the chemical processes occurring within the incineration equipment. A detailed chemical kinetic mechanism for combustion of the nerve agent GB has been developed⁶, but no kinetics or thermochemistry existed previously for modeling combustion of HD or the nerve agent VX.

Combustion or thermal reaction of HD in the presence of oxygen to convert it into the products CO_2 , HCl , SO_2 (or H_2SO_4) and H_2O is one method that can be used effectively to destroy the mustard agent. The combustion or oxidation process, however needs to completely destroy the agent and its immediate decomposition products. The thermal reactions of mustard or any hydrocarbon sulfide, include pyrolysis (unimolecular decomposition), as well as reactions with the radical pool to effect hydrocarbon and sulfur radicals of the bis(2-chloroethyl) sulfide. These radicals then react with oxygen molecules and oxygen-containing radical species (O , OH , HO_2 , CH_3O , etc.), eventually converting to lower energy products, as noted above.

Sulfur species are also present in many fuels, including coals, heating oil, aircraft fuels, and diesel and gasoline. In all these cases the source of fuel sulfur is contact of the elemental forms of sulfur with the natural underground deposits, where sulfur becomes incorporated into the gas and crude oil stocks. A significant fraction of the sulfur in these liquid fuels is removed prior to use (combustion) in order to prevent pollution of the air, formation of SO_2 and subsequent formation of particulates and acid rain. It is more difficult to remove the sulfur from coals; but this is performed in many cases as well. Sulfur does persist in these cleaned fuels and oils that are treated for its removal to some extent and the sulfur species are subsequently combusted in their use.

In plants and animals, sulfur occurs in various proteins, and it is one of the 10 most abundant elements in the human body.⁷ Sulfur compounds are present and of interest in biological systems, in atmospheric chemistry, and in environmental science. The known involvement of sulfur-centered radicals in these biological systems suggests that knowledge on the fundamental thermodynamic properties of the sulfur moieties would be valuable in understanding its effects on these systems.⁸

The knowledge and understanding the oxidation and thermal reactivity of these sulfur species requires their thermodynamic properties, bond energies and kinetic parameters for unimolecular reactions to be known.

The use of Density Functional Theory, B3LYP/6-31g(d,p), with isodesmic working reactions for enthalpy of formation of sulfur hydrocarbons is tested in this study using a set of known sulfur hydrocarbons. Satisfactory results (below) indicate that we can use this computational chemistry method to determine thermochemical properties and kinetics. This part I of our study focuses on unimolecular (thermal) reactions of the mustard and on its thermochemistry for evaluation of initial abstraction reactions that result in the initial radical products. These radical intermediates react, as noted above, with oxygen species and by further unimolecular decomposition processes.

Thermodynamic properties for reactants, transition states, and products from unimolecular dissociations of $\text{CH}_3\text{CH}_2\text{SCH}_2\text{CH}_3$, $\text{CH}_3\text{CH}_2\text{SCH}_2\text{CH}_2\text{Cl}$, and $\text{CH}_2\text{ClCH}_2\text{SCH}_2\text{CH}_2\text{Cl}$ and for their radicals resulting from bond cleavage reactions are analyzed. $\Delta_f H^\circ_{298}$ for the molecules and radicals are determined using isodesmic reaction analysis at the B3LYP/6-31G(d,p) level, with S°_{298} and $C_p(T)$ determined using geometric parameters and vibrational frequencies obtained at this same level of theory. Potential barriers for the internal rotor potentials are also calculated at the B3LYP/6-31G(d,p) level, and the hindered rotation contributions to S°_{298} and $C_p(T)$ are calculated. A more limited number of studies, specifically for transition states are also performed at KMLYP/6-311G(d,p), CBS-Q, and CBS-QB3 levels of theory, with the CBS-QB3 barriers recommended. Hydrogen bond dissociation energies of CH_3SH , $\text{CH}_3\text{CH}_2\text{SH}$, CH_3SCH_3 , $\text{CH}_3\text{CH}_2\text{SCH}_2\text{CH}_3$, and $\text{CH}_3\text{CH}_2\text{SCH}_2\text{CH}_2\text{Cl}$ are calculated and compared with literature values where available. Four center (Retro-ene like) reactions and C—S bond dissociations are important initial decomposition channels in the hydrocarbon–sulfur moieties.

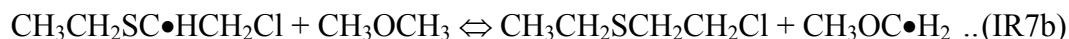
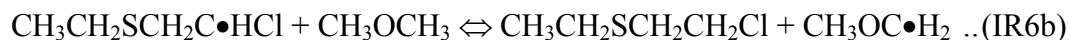
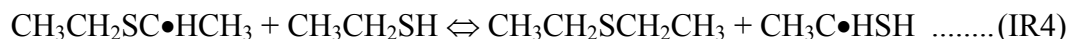
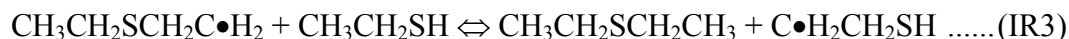
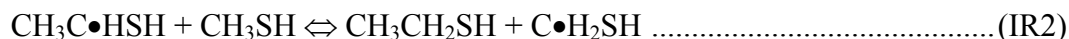
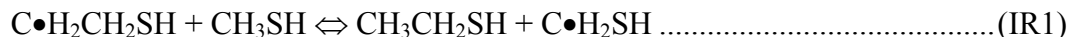
Calculation Method

Geometries and Vibration Frequencies The initial structures of reactants, transition states and products are determined using ROHF or UHF/PM3 in MOPAC,⁹ followed by optimization and vibrational frequency calculation at B3LYP/6-31G(d,p) level using GAUSSIAN 98.¹⁰ Transition state geometries are identified by the existence of only one imaginary frequency, structure information, and the transition state theory reaction coordinate vibration information. Zero-point vibrational energies are scaled by 0.9806 as recommended by Scott and Radom.¹¹ Geometries of transition states optimized at B3LYP/6-31G(d,p) are shown in Figure 1.

Enthalpies of Formation We evaluated enthalpies of formation ($\Delta_f H^\circ_{298}$) at B3LYP/6-31G(d,p) level on several sulfur hydrocarbons and corresponding radicals with a method of isodesmic reaction and show that the B3LYP/6-31G(d,p) values are in agreement with accepted literature

values in Table 1. The evaluated $\Delta_f H^\circ_{298}$ for the reference molecules and radicals in the isodesmic reactions are given in Table 2.

Enthalpies of formation for reactants and products are calculated at B3LYP/6-31G(d,p) level. The method of isodesmic reactions for $\text{C}\cdot\text{H}_2\text{CH}_2\text{SH}$, $\text{CH}_3\text{C}\cdot\text{HSH}$, $\text{CH}_3\text{CH}_2\text{SCH}_2\text{C}\cdot\text{H}_2$, $\text{CH}_3\text{CH}_2\text{SC}\cdot\text{HCH}_3$, $\text{CH}_3\text{CH}_2\text{SCH}_2\text{CH}_2\text{Cl}$, $\text{CH}_3\text{CH}_2\text{SCH}_2\text{C}\cdot\text{HCl}$, and $\text{CH}_3\text{CH}_2\text{SC}\cdot\text{HCH}_2\text{Cl}$ is used to determine for accurate enthalpies of formation at B3LYP/6-31G(d,p) and recently published KMLYP density functional method with the /6-311G(d,p) basis set.¹² The evaluated reaction enthalpies and enthalpies of formation in the isodesmic reactions are listed in Table 3.



Enthalpies of formation for transition states Although B3LYP has achieved good success in predicting thermochemistry of molecules, several studies report that B3LYP is less accurate for predicting barriers and has a tendency to underestimate barriers.¹²⁻¹⁵ We performed further calculations for barriers with four different methods (B3LYP/6-31G(d,p), KMLYP/6-311G(d,p)¹², CBS-Q¹⁶⁻¹⁸, and CBS-QB3^{19,20}). Comparison of barriers is given in Table 4. The barrier is calculated relative to the reactants. The complete basis set (CBS-QB3) method of Montgomery et al.^{19,20} for computing accurate energies is used to determine the activation energies used in our kinetic analysis.

Entropy and Heat Capacity The contributions of external rotations, translations, and vibrations to entropies and heat capacities are calculated from scaled vibration frequencies and moments of inertia for the optimized B3LYP/6-31G(d,p) structures. The number of optical isomers and spin degeneracy of unpaired electrons are also incorporated. Contributions from hindered internal rotation for S and $C_p(T)$ are determined using direct integration over energy levels of the intramolecular rotational potential curves. A program, ROTATOR²¹, is used for calculation of the energy levels. This technique employs expansion of the hindrance potential in the Fourier series (E1), calculation of the Hamiltonian matrix on the basis of wave functions of the free internal rotor, and subsequent calculation of energy levels by direct diagonalization of the

Hamiltonian matrix.²²⁻²⁴ The torsional potential calculated at discrete torsion angles is represented by a truncated Fourier series:

$$V(\Phi) = a_0 + \sum a_i \cos(i\Phi) + \sum b_i \sin(i\Phi) \quad i = 1, 2, 3, \dots \quad (\text{E1})$$

Values of the coefficients (a_0 , a_i and b_i) are calculated to provide the minimum and maximum of the torsional potentials with allowance of a shift of the theoretical extreme angular positions²²⁻²⁴. The energy levels are used to determine partition coefficients and their contributions to S and $C_p(T)$ through relationships from statistical mechanics.

High-Pressure Limit Pre-exponential Factors and Rate Constants For the reactions where thermochemical properties of transition states are calculated by *ab initio* or density functional methods, k_∞ 's are fit by three parameters A , n , and Ea over temperature range from 298 to 2000K, $k_\infty = A(T)^n \exp(-Ea/RT)$. Entropy differences between reactant and transition state are used to determine the pre-exponential factor, A , via canonical Transition State Theory (TST)

$$A = (k_b T / h_p) \exp(\Delta S^\ddagger / R), \quad Ea = \Delta H^\ddagger$$

Where h_p is the Planck constant and k_b is the Boltzmann constant. Treatment of the internal rotors for S and $C_p(T)$ is important here because these internal rotors are often lost in the cyclic transition state structures.

Results and Discussion

Rotational Barriers Potential barriers for internal rotations of $\text{CH}_3\text{CH}_2\text{SCH}_2\text{CH}_2\text{Cl}$ and $\text{CH}_2\text{ClCH}_2\text{SCH}_2\text{CH}_2\text{Cl}$ are calculated in the B3LYP/6-31G(d,p) level and shown in Figures 2 and 3, respectively. The potential energies are calculated as a function of the dihedral angle by varying the torsion angle in 30° intervals and allowing other parameters to be optimized. The barriers for internal rotations are calculated from the differences between the total energy of each conformation and that of the most stable conformer at 0 K, where the zero point vibrational energy (ZPVE) and thermal correction to 298 K are not included. Total energies at 0 K and calculated internal rotation barriers versus the dihedral angle are presented in the coefficients of the Fourier expansion components, a_i , and b_i in equation E1.

Entropy (S°_{298}) and Heat Capacity ($C_p(T)$) S°_{298} and $C_p(T)$'s are calculated based on scaled vibration frequencies and moments of inertia of the optimized B3LYP/6-31G(d,p) structures. The calculation results are summarized in Table 5. TVR represents the sum of the contributions from translation, vibrations and external rotations for $S^\circ_{(298)}$ and $C_p(T)$'s. Symmetry, number of optical isomers and electronic spin are incorporated in estimation of $S^\circ_{(298)}$ as described in Table 5. Torsion frequencies are omitted in these calculations, instead, contributions from internal rotation for $S^\circ_{(298)}$ and $C_p(T)$'s are determined using direct integration over energy levels of the intramolecular rotational potential curves¹⁴⁻¹⁶ and noted in Table 5.

Hydrogen bond dissociation energies in CH_3SH , $\text{CH}_3\text{CH}_2\text{SH}$, CH_3SCH_3 , $\text{CH}_3\text{CH}_2\text{SCH}_2\text{CH}_3$, and $\text{CH}_3\text{CH}_2\text{SCH}_2\text{CH}_2\text{Cl}$ Hydrogen bond dissociation energies (BDEs) for the C—H and S—H bonds in CH_3SH , $\text{CH}_3\text{CH}_2\text{SH}$, CH_3SCH_3 , $\text{CH}_3\text{CH}_2\text{SCH}_2\text{CH}_3$, and $\text{CH}_3\text{CH}_2\text{SCH}_2\text{CH}_2\text{Cl}$ are presented in Table 6. Our calculation results at B3LYP/6-31G(d,p) level of theory are compared

with literature values when available. If not, the values of KMLYP density functional method with the /6-311G(d,p) basis set are compared. For alkyl RSH species Lias et al.²⁵ and Griller et al.²⁶ agreed that BDE(S—H) was effectively independent of the structure of the R group. This was based on values of BDE derived from the electron affinities of the RS radicals and the $\Delta H_{\text{acid}}^\circ$ values of the molecules. They recommended a value of 87.00 ± 2.15 kcal/mole²⁵ and 88.43 ± 1.91 kcal/mol²⁶, respectively, for BDE(S—H). Amstrong⁶ also reported BDE(S—H) value for all the RSH species is 87.47 ± 0.96 kcal/mol. Our calculation values are ~ 89 kcal/mol for CH₃S—H and CH₃CH₂S—H. We determine the BDEs of H—CH₂SH (96.3) and H—CH₂SCH₃ (95.4) are about 2 kcal/mol higher than literature values. (93.9 and 93.3 kcal/mol, respectively.^{25,27-29}) The corresponding hydrogen BDEs for CH₃CH₂SH, CH₃CH₂SCH₂CH₃, and CH₃CH₂SCH₂CH₂Cl are reported in Table 6.

Unimolecular Dissociation Reactions of CH₃CH₂SCH₂CH₃, CH₃CH₂SCH₂CH₂Cl, and CH₂ClCH₂SCH₂CH₂Cl Potential energy diagrams for unimolecular dissociations of CH₃CH₂SCH₂CH₃, CH₃CH₂SCH₂CH₂Cl, and CH₂ClCH₂SCH₂CH₂Cl are illustrated in Figure 4.

Retro-ene Reaction CH₃CH₂SCH₂CH₃ can dissociate to CH₃CH₂SH + C₂H₄ via a four-center hydrogen shift transition state (TS1). This reaction, when involving a six-member ring, is often termed a retro-ene reaction and we use this terminology through the rest of this manuscript. TS1 structure is illustrated in Figure 1(a). The H6 atom is in a bridge structure shifting from C5 to S3. The cleaving C5-H6 bond is 1.28Å and the forming S3-H6 bond is 1.75Å. The cleaving S3-C4 bond is 2.69Å. All structures are from B3LYP/6-31G(d,p) determined geometries. The barrier is 64.41 kcal/mol is some 20 kcal/mol higher than a conventional 6 center retro-ene reaction due to strain in the four-center ring strain of the transition state.

CH₃CH₂SCH₂CH₂Cl can dissociate to CH₃CH₂SH + CH₂CHCl or CH₃CH₂SCl + C₂H₄ via a hydrogen or a chlorine atom shift (TS2B or TS2C), where transition state structures are illustrated in Figures 1(c) and 1(d), respectively. The latter reaction (TS2C) with a chlorine shift has an ~ 11 kcal/mol higher barrier than TS2B which has a hydrogen shift. (78.61 and 67.77 kcal/mol barriers for TS2C and TS2B, respectively.) This is a result of the weak S—Cl bond being formed, relative to the S—H bond.

CH₂ClCH₂SCH₂CH₂Cl also can undergo a dissociation to CH₂ClCH₂SH + CH₂CHCl or CH₂ClCH₂SCl + C₂H₄ via a hydrogen or a chlorine shift (TS3B or TS3C), where Figures 1(f) and 1(g) show transition state structures, respectively. The optimized geometries of TS3B and TS3C and barriers of 66.99 and 77.64 kcal/mol in these reactions are very similar to the optimized geometries of the respective reactions of TS2B and TS2C and 67.77 and 78.61 kcal/mol barriers for CH₃CH₂SCH₂CH₂Cl.

HCl Elimination CH₃CH₂SCH₂CH₂Cl can dissociate to CH₃CH₂SCH=CH₂ + HCl via HCl elimination (TS2A) with a 57.27 kcal/mol barrier, which is ~ 10 and 21 kcal/mol lower than the 4 center hydrogen and chlorine shift reactions (TS2B or TS2C), respectively. The TS2A structure is illustrated in Figure 1(b). The leaving C4-H9 and C5-Cl6 bonds are 1.25 and 2.61Å, respectively.

$\text{CH}_2\text{ClCH}_2\text{SCH}_2\text{CH}_2\text{Cl}$ also can undergo dissociation to $\text{CH}_2\text{ClCH}_2\text{SCH}=\text{CH}_2 + \text{HCl}$ via HCl elimination (TS3A). The optimized geometry of TS3A and a barrier of 59.11 kcal/mol in this reaction are very similar to the optimized geometry of TS2A and 57.27 kcal/mol barrier in $\text{CH}_3\text{CH}_2\text{SCH}_2\text{CH}_2\text{Cl}$ reaction with only one Cl in the dithiol molecule. Figure 1(e) shows transition state structure. The leaving C4-H9 and C5-Cl6 bonds are 1.26 and 2.60 Å, respectively.

Bond Cleavage Reaction Bond dissociation energies of $\text{CH}_3\text{CH}_2\text{SCH}_2\text{CH}_3$ and $\text{CH}_3\text{CH}_2\text{SCH}_2\text{CH}_2\text{Cl}$ are illustrated in Figure 5. $\text{CH}_3\text{CH}_2\text{SCH}_2\text{CH}_3$ can undergo bond cleavage reactions to $\text{CH}_3\text{CH}_2\text{S}\bullet + \text{C}_2\text{H}_5$ or $\text{CH}_3\text{CH}_2\text{SCH}_2\bullet + \text{CH}_3$ with barriers of 73.02 or 83.95 kcal/mol, respectively. $\text{CH}_3\text{CH}_2\text{SCH}_2\text{CH}_2\text{Cl}$ can undergo similar bond cleavage reactions to $\text{CH}_3\text{CH}_2\text{S}\bullet + \text{C}\bullet\text{H}_2\text{CH}_2\text{Cl}$ or $\text{CH}_3\text{CH}_2\text{SCH}_2\bullet + \text{CH}_2\text{Cl}$ with 74.42 or 83.20 kcal/mol barriers, respectively. $\text{CH}_3\text{CH}_2\text{SCH}_2\text{CH}_2\text{Cl}$ also can undergo dissociation to $\text{CH}_3\text{CH}_2\text{SCH}_2\text{CH}_2\bullet + \text{Cl}$ with a barrier of 80.45 kcal/mol. Hydrogen BDEs for $\text{CH}_3\text{CH}_2\text{SCH}_2\text{CH}_3$ and $\text{CH}_3\text{CH}_2\text{SCH}_2\text{CH}_2\text{Cl}$ were discussed previously.

Thermodynamic and Kinetic Analysis of Unimolecular Dissociation Reactions Thermodynamic and kinetic analysis on the unimolecular dissociation of $\text{CH}_3\text{CH}_2\text{SCH}_2\text{CH}_3$, $\text{CH}_3\text{CH}_2\text{SCH}_2\text{CH}_2\text{Cl}$, and $\text{CH}_2\text{ClCH}_2\text{SCH}_2\text{CH}_2\text{Cl}$.

Multifrequency quantum Rice-Ramsperger-Kassel (QRRK) calculations^{30,31} for $k(E)$ and modified strong collision analysis of Gilbert et al.³²⁻³⁴ for falloff are performed on this reaction system to estimate rate constants and to determine important reaction paths as a function of temperature. All dissociation paths are pressure-independent above 0.01 atm. Plots of rate constants at 1 atm. versus $1000/T$ for unimolecular dissociations of $\text{CH}_3\text{CH}_2\text{SCH}_2\text{CH}_3$, $\text{CH}_3\text{CH}_2\text{SCH}_2\text{CH}_2\text{Cl}$, and $\text{CH}_2\text{ClCH}_2\text{SCH}_2\text{CH}_2\text{Cl}$ are given in Figure 6, 7 and 8, respectively.

For $\text{CH}_3\text{CH}_2\text{SCH}_2\text{CH}_3$ dissociation, bond cleavage reactions to $\text{CH}_3\text{CH}_2\text{S}\bullet + \text{C}_2\text{H}_5$ is most important above 800 K. $\text{CH}_3\text{CH}_2\text{SH} + \text{C}_2\text{H}_4$ via TS1 and $\text{CH}_3\text{CH}_2\text{SCH}_2\bullet + \text{CH}_3$ products have two orders of magnitude lower rate constants than C—S bond cleavage reaction above 1500 K.

For the unimolecular dissociations of $\text{CH}_3\text{CH}_2\text{SCH}_2\text{CH}_2\text{Cl}$ and $\text{CH}_2\text{ClCH}_2\text{SCH}_2\text{CH}_2\text{Cl}$, HCl eliminations (TS2A or TS3A) are most important channel at high and low temperatures. Carbon–sulfur and carbon–chlorine bond cleavage reactions become important at higher temperatures (above 1000 K), because of higher Arrhenius pre-exponential factors.

Reaction Mechanism

Thermodynamic data and kinetics generated in this work were combined with existing mechanisms for combustion chemistry of chlorine^{35,36}, sulfur³⁷, and nitrogen and hydrocarbon chemistry³⁸. The resulting detailed chemical kinetic mechanism models the complete oxidation and pyrolysis process for HD and other chlorosulfides.

Sensitivity Analysis Using this detailed kinetic mechanism, normalized first order sensitivity coefficients were calculated in a perfectly stirred reactor (PSR) code for a variety of inlet compositions, temperatures, and reactor residence times to determine the main destruction pathways for HD.

Sensitivity analysis was conducted under the following conditions, chosen to approximate those that might be found in an incinerator: 1) 1000 ppm HD in air, 2) a fuel-rich (equivalence ratio = 3.0) mixture of HD and air, 3) 1000 ppm of HD in equilibrium fuel lean (equivalence ratio = 0.8) methane-air products, and 4) 1000 ppm of HD in fuel lean (equivalence ratio = 0.8) methane-air products with major species (H_2O , O_2 , CO , CO_2 , N_2) in equilibrium and with superequilibrium concentrations of H, O, OH, and Cl radicals. The superequilibrium radical concentrations for the radicals were chosen as the peak values from a series of PSR calculations in which the residence time was varied. The analysis was conducted for residence times from 10^{-6} to 1000 sec. and temperatures of 1000, 1250, 1500, 1750, and 2000 K.

It was found that under almost all conditions that destruction of the HD molecule is dominated by the HCl elimination pathway described above. The only exception to this is for HD in air, at low temperatures (less than about 1250 K) and high Cl atom concentrations, where H abstraction by Cl is the dominant pathway. For HD mixed with methane-air products, HCl elimination was always the dominant pathway. Key results of the sensitivity analysis are shown in Figures 9 and 10.

Summary

Thermodynamic properties for reactants, transition states and products for the unimolecular dissociation of $\text{CH}_3\text{CH}_2\text{SCH}_2\text{CH}_3$, $\text{CH}_3\text{CH}_2\text{SCH}_2\text{CH}_2\text{Cl}$, and $\text{CH}_2\text{ClCH}_2\text{SCH}_2\text{CH}_2\text{Cl}$ are calculated at the B3LYP/6-31G(d,p) level. $\Delta_f H^\circ_{298}$ values are determined with isodesmic reactions. S°_{298} and $C_p(T)$ are determined using geometric parameters and vibrational frequencies obtained at the B3LYP/6-31G(d,p). The hindered rotational contributions to S°_{298} and $C_p(T)$ are calculated by intramolecular torsion potential curves. Hydrogen bond dissociation energies of CH_3SH , $\text{CH}_3\text{CH}_2\text{SH}$, CH_3SCH_3 , $\text{CH}_3\text{CH}_2\text{SCH}_2\text{CH}_3$, and $\text{CH}_3\text{CH}_2\text{SCH}_2\text{CH}_2\text{Cl}$ are calculated at the B3LYP/6-31G(d,p). For $\text{CH}_3\text{CH}_2\text{SCH}_2\text{CH}_3$ dissociation, bond cleavage reactions to $\text{CH}_3\text{CH}_2\text{S}\bullet + \text{C}_2\text{H}_5$ is most important at higher temperature (above 800 K). For the unimolecular dissociations of $\text{CH}_3\text{CH}_2\text{SCH}_2\text{CH}_2\text{Cl}$ and $\text{CH}_2\text{ClCH}_2\text{SCH}_2\text{CH}_2\text{Cl}$, HCl eliminations via TS2A and TS3A, respectively, are the most important channel at high and low temperatures.

Acknowledgements

Funding for this project was provided through a DoD-Army Phase II SBIR, "Engineering Design Software for Military Incinerators", contract number DAAD19-01-C-0050, Program Official Dr. Robert Shaw (Army Research Office). We acknowledge the USEPA Northeast Regional Research Center and the USEPA Airborne Organics Research Center for partial funding. Thanks to Dr. C. Sheng for the SMCPS program and Mr. Randall Nelson for help with the sensitivity calculations.

References

1. Lapp, R. R. and Schneider, C. J. Jr., "An Investigation of the Thermal Decomposition of Bis (2, Ethyl Hexyl) Hydrogen Phosphite and Agent VX as Vapor at Elevated Temperatures," Cornell Aeronautical Laboratories Report No. GM-1592-G-5, Contract No. DA-18-108-CML-6628, 1962.
2. Brooks, M.E. and Parker, G.A., "Incineration/Pyrolysis of Several Agents and Related Chemical Materials Contained in Identification Sets," Technical Report ARCSL-TR-79040, US Army Toxic and Hazardous Materials Agency, Aberdeen Proving Ground, Maryland, October, 1979.

3. Montgomery, C. J., Bockelie, M. J., Sarofim, A. F., Magee, R. S., Gouldin, F. C., Bozzelli, J. W., and Westbrook, C. K., "Chemical Agent Decomposition Rates at Temperatures Anticipated in the Discharge Airlock," Reaction Engineering International Project No. 4440, Feb 20, 2003.
4. Gouldin, F. C., and Fisher, E. M., "Incineration and Thermal Treatment of Chemical Agents and Chemical Weapons," in *Emerging Technologies in Hazardous Waste Management* 7, pp. 33-47, Plenum Press, 1997.
5. Denison, M. K., Montgomery, C. J., Sarofim, A. F., Bockelie, M. J., and Webster, A. G., "Computational Modeling of a Chemical Demilitarization Deactivation Furnace System," Twenty-Second International Conference on Incineration and Thermal Treatment Technologies, Orlando, FL, May 12-16, 2003.
6. Glaude, P.A., Melius, C., Pitz, W.J., and Westbrook, C.K., "Detailed Chemical Kinetic Reaction Mechanism for Incineration of Organophosphorus and Fluoro-Organophosphorus Compounds," *Proceedings of the Combustion Institute*, Vol. 29, pp. 2469-2476, 2002.
7. McMurry, J.; Fay, R. C. Chemistry, Prentice-Hall, Upper Saddle River, US, 2001.
8. Armstrong, D. A. *S-centered radicals*; Wiley: Chichester, UK, 1999; Chapter 2.
9. Stewart, J. J. P. *MOPAC 6.0*, Frank J. Seiler Research Laboratory, U.S. Air Force Academy: Colorado Spring, CO, 1990.
10. Frisch, M. J.; Trucks, G. W.; Schlegel, H. B.; Scuseria, G.; Robb, M. A.; Cheesman, J. R.; Zakrzewski, V. G.; Montgomery, J. A., Jr.; Stratmann, R. E.; Burant, J. C.; Dapprich, S.; Millam, J. M.; Daniels, A. D.; Kudin, K. N.; Strain, M. C.; Farkas, O.; Tomasi, J.; Barone, V.; Cossi, M.; Cammi, R.; Mennucci, B.; Pomelli, C.; Adamo, C.; Clifford, S.; Ochterski, J.; Petersson, G. A.; Ayala, P. Y.; Cui, Q.; Morokuma, K.; Malick, D. K.; Rabuck, A. D.; Raghavachari, K.; Froesman, J. B.; Cioslowski, J.; Ortiz, J. V.; Baboul, A. G.; Stefanov, R. B.; Liu, G.; Liashenko, A.; Piskorz, P.; Komaromi, I.; Gomperts, R.; Matrin, R. L.; Fox, D. J.; Keith, T.; Al-Laham, M. A.; Peng, C. Y.; Nanayakkara, A.; Gonzalez, C.; Challacombe, M.; Gill, P. M. W.; Johnson, B.; Chen, W.; Wong, M. W.; Andres, J. L.; Head-Gordon, M.; Pople, J. A. *Gaussian 98*; Gaussian Inc.: Pittsburgh, PA, 1998.
11. Scott, A. P.; Radom, L. *J. Phys. Chem.* 1996, 100, 16502.
12. Kang, J. K.; Musgrave, C. B. *J. Chem. Phys.* 2001, 115, 11040.
13. Zhang, Y. K.; Yang, W. T. *J. Chem. Phys.* 1998, 109, 2604.
14. Johnson, B. G.; Gonzales, C. A.; Gill, P. M. W.; Pople, J. A. *Chem. Phys. Lett.* 1994, 221, 100.
15. Jursic, B. S. *Chem. Phys. Lett.* 1996, 256, 603.
16. Petersson, G. A.; Tensfeldt, T. G.; Montgomery, J. A., Jr. *J. Chem. Phys.* 1991, 94, 6091.
17. Ochterski, J. W.; Petersson, G. A.; Wiberg, K. *J. Am. Chem. Soc.* 1995, 117, 11299.
18. Ochterski, J. W.; Petersson, G. A.; Montgomery, J. A., Jr. *J. Chem. Phys.* 1996, 104, 2598.
19. Montgomery, J. A., Jr.; Frisch, M. J.; Ochterski, J. W.; Petersson, G. A.; *J. Chem. Phys.* 1999, 110, 2822.
20. Montgomery, J. A., Jr.; Frisch, M. J.; Ochterski, J. W.; Petersson, G. A.; *J. Chem. Phys.* 2000, 112, 6532.
21. Shokhirev, N. V. <http://www.chem.arizona.edu/faculty/walk/nikolai/programs.html#programs>
22. Lay, T. H.; Krasnoperov, L. N.; Venanzi, C. A.; Bozzelli, J. W. *J. Phys. Chem.* 1996, 100, 8240.
23. Yamada, T.; Lay, T. H.; Bozzelli, J. W. *J. Phys. Chem. A* 1998, 102, 7286.
24. Yamada, T.; Lay, T. H.; Bozzelli, J. W. *J. Phys. Chem. A* 1999, 103, 5602.
25. Lias, S. G.; Bartmess, J. E.; Liebman, J. F.; Holmes, J. L.; Levin, R. D.; Mallard, W.G. *J. Phys. Chem. Ref. Data* 1988, 17, Supplement No.1.
26. Griller, D.; Martinho Simoes, J. A.; Wayner, D. D. M. *Sulfur-Centered Reactive Intermediates in Chemistry and Biology*; Chatgililoglu, C., Asmus, K. D., Eds.; Nato ASI Series, Plenum: New York, 1990; pp 37-52.
27. Ruscic, B.; Berkowitz, J. *J. Chem. Phys.* 1992, 97, 1818.
28. Nourbakhsh, S.; Norwood, K.; Yin, H. M.; Liao, C. L.; Ng, C. Y. *J. Chem. Phys.* 1991, 95, 5014.
29. Jefferson, A.; Nicovich, J. M.; Wine, P. H. *J. Phys. Chem.* 1994, 98, 7128.
30. Chang, A. Y.; Bozzelli, J. W.; Dean, A. M. *Int. J. Res. Phys. Chem. Chem. Phys. (Zeit. Phys. Chem)* 2000, 214, 1533.

31. Sheng, C. Y.; Bozzelli, J. W.; Dean, A. M.; Chang, A. Y. *J. Phys. Chem. A* 2002, 106, 7276.
32. Gilbert, R. G.; Smith, S. C. *Theory of Unimolecular and Recombination Reactions*; Oxford Press: New York, 1990.
33. Gilbert, R. G.; Smith, S. C.; Jordan, M. J. T. *UNIMOL Program Suite (Calculation of Fall-off Curve for Unimolecular and Recombination Reactions)*, Sidney, 1993.
34. Gilbert, R. G.; Luther, K.; Troe, J. *Ber. Bunsen-Ges. Phys. Chem.* 1983, 87, 169.
35. Ho, W.; Booty, M. R.; Magee, R. S., and Bozzelli, J. W., *Ind. Eng. Chem. Res.* 34:4185-4192, 1995.
36. Procaccini, C., Bozzelli, J. W., Longwell, J. P., Smith, K. A., and Sarofim, A. F., *Environmental Science and Technology* 34:4565-4570, 2000.
37. Nimmo, W., Hampartsoumian, E., Hughes, K. J., and Tomlin, A. S., "Experimental and Kinetic Studies on the Effect of Sulfur-Nitrogen Interactions on NO Formation in Flames," *Twenty-Seventh Symposium (International) on Combustion*, pp. 1419-1426, 1998.
38. Dean, A.M., and Bozzelli, J.W., "Combustion Chemistry of Nitrogen," in *Gas-Phase Combustion Chemistry*, Gardiner, W.C., ed., Springer, pp. 125-341, 1999.

Species Name & Structure	Bond Length (Å)		Bond Angle (Degree)		Dihedral Angle (Degree)	
[a] TS1	r21		1.53			
	r32		1.84			
	r43		2.69		∠321	114.9
	r54		1.40		∠432	166.9
	r65		1.28		∠4321	96.0
	r75		1.09		∠543	78.1
	r85		1.09		∠5431	-104.3
	r94		1.08		∠654	100.8
	r104		1.08		∠6543	0.4
	r112		1.10		∠754	117.1
	r122		1.10		∠7543	-108.7
	r131		1.10		∠854	117.1
	r141		1.09		∠8543	109.2
	r151		1.09		∠943	96.6
					∠9436	-121.3
					∠1043	96.9
					∠10436	120.5
					∠1121	111.3
					∠11213	-122.3
[b] TS2A	r21		1.53			
	r32		1.85			
	r43		1.80		∠321	109.4
	r54		1.40		∠432	100.6
	r65		2.61		∠4321	176.0
	r75		1.08		∠543	119.8
	r85		1.08		∠5432	134.1
	r94		1.25		∠654	90.7
	r104		1.09		∠6543	-106.5
	r112		1.09		∠754	121.1
	r122		1.09		∠7543	161.8
	r131		1.09		∠854	121.3
	r141		1.09		∠8543	-16.7
	r151		1.09		∠943	109.2
					∠9432	45.3
					∠1043	117.0
					∠10432	-74.5
					∠1121	111.3
					∠11213	-119.5
[c] TS2B	r21		1.53			
	r32		1.84			
	r43		2.64		∠321	114.9
	r54		1.40		∠432	165.4
	r65		1.29		∠4321	95.9
	r75		1.79		∠543	78.4
	r85		1.09		∠5431	-108.9
	r94		1.08		∠654	100.4
	r104		1.08		∠6543	1.9
	r112		1.10		∠754	118.1
	r122		1.10		∠7543	-110.5
	r131		1.10		∠854	118.1
	r141		1.09		∠8543	111.1
	r151		1.09		∠943	99.9
					∠9436	-122.4
					∠1043	94.4
					∠10436	117.8
					∠1121	111.6
					∠11213	-122.0

Figure 1. Geometries of Transition States Optimized at B3LYP/6-31G(d,p).

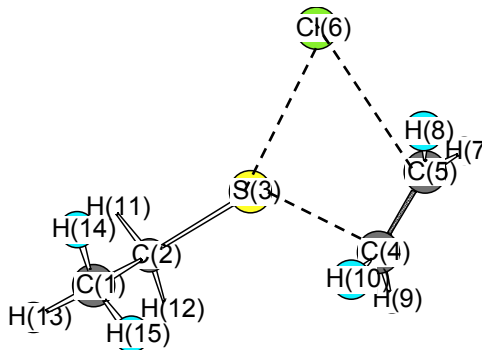
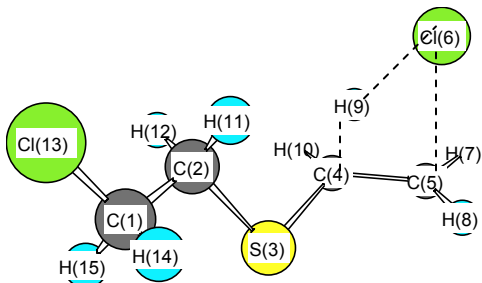
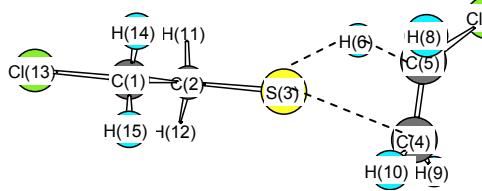
Species Name & Structure	Bond Length (Å)		Bond Angle (Degree)		Dihedral Angle (Degree)	
[d] TS2C						
	r21	1.53				
	r32	1.84	∠321	116.2		
	r43	2.30	∠432	125.3	∠4321	73.2
	r54	1.38	∠543	95.3	∠5431	179.9
	r63	2.66	∠632	141.2	∠6321	-107.0
	r75	1.08	∠754	121.4	∠7543	-91.1
	r85	1.08	∠854	121.4	∠8543	91.3
	r94	1.09	∠943	97.8	∠9432	59.1
	r104	1.09	∠1043	98.0	∠10432	-59.4
	r112	1.10	∠1121	111.1	∠11213	-115.4
	r122	1.10	∠1221	112.7	∠12213	126.8
	r131	1.10	∠1221	110.7	∠12213	175.6
	r141	1.09	∠1312	111.0	∠13123	55.3
	r151	1.09	∠1412	111.2	∠14123	-64.8
				∠1512	∠15123	
[e] TS3A						
	r21	1.52				
	r32	1.85	∠321	108.2		
	r43	1.80	∠432	99.9	∠4321	175.2
	r54	1.41	∠543	119.4	∠5432	134.6
	r65	2.60	∠654	90.4	∠6543	-106.3
	r75	1.08	∠754	120.9	∠7543	161.7
	r85	1.08	∠854	121.4	∠8543	-16.5
	r94	1.26	∠943	109.3	∠9432	45.4
	r104	1.09	∠1043	116.8	∠10432	-74.7
	r112	1.09	∠1121	110.9	∠11213	-119.6
	r122	1.09	∠1121	110.4	∠12213	119.2
	r131	1.81	∠1221	110.2	∠12213	-179.1
	r141	1.09	∠1312	111.8	∠13123	62.5
	r151	1.09	∠1412	111.8	∠14123	-60.5
				∠1512	∠15123	
[f] TS3B						
	r21	1.52				
	r32	1.84	∠321	111.7		
	r43	2.65	∠432	166.1	∠4321	94.0
	r54	1.40	∠543	78.4	∠5431	-112.0
	r65	1.29	∠654	100.3	∠6543	2.0
	r75	1.78	∠754	118.2	∠7543	-110.3
	r85	1.09	∠854	118.0	∠8543	111.0
	r94	1.08	∠943	99.9	∠9436	-122.6
	r104	1.08	∠1043	94.1	∠10436	117.7
	r112	1.09	∠1121	111.3	∠11213	-120.9
	r122	1.09	∠1121	111.1	∠12213	119.9
	r131	1.83	∠1221	111.1	∠12213	-179.7
	r141	1.09	∠1312	111.7	∠13123	61.7
	r151	1.09	∠1412	111.7	∠14123	-61.0
				∠1512	∠15123	

Figure 1. Geometries of Transition States Optimized at B3LYP/6-31G(d,p) (continued).

Species Name & Structure	Bond Length (Å)		Bond Angle (Degree)		Dihedral Angle (Degree)	
	r21	1.52				
	r32	1.85	∠321	115.9		
	r43	2.28	∠432	124.5	∠4321	73.1
	r54	1.39	∠543	95.3	∠5431	-179.0
	r63	2.64	∠632	140.5	∠6321	-106.5
	r75	1.08	∠754	121.5	∠7543	-91.9
	r85	1.08	∠854	121.4	∠8543	89.9
	r94	1.09	∠943	98.4	∠9432	60.3
	r104	1.09	∠1043	97.1	∠10432	-58.0
	r112	1.10	∠1121	109.0	∠11213	-114.9
	r122	1.09	∠1221	111.9	∠12213	127.7
	r131	1.09	∠1312	111.5	∠13123	173.1
	r141	1.09	∠1412	111.6	∠14123	49.8
	r151	1.82	∠1412	111.3	∠14123	-68.9
			∠1512		∠15123	

Figure 1. Geometries of Transition States Optimized at B3LYP/6-31G(d,p) (continued).

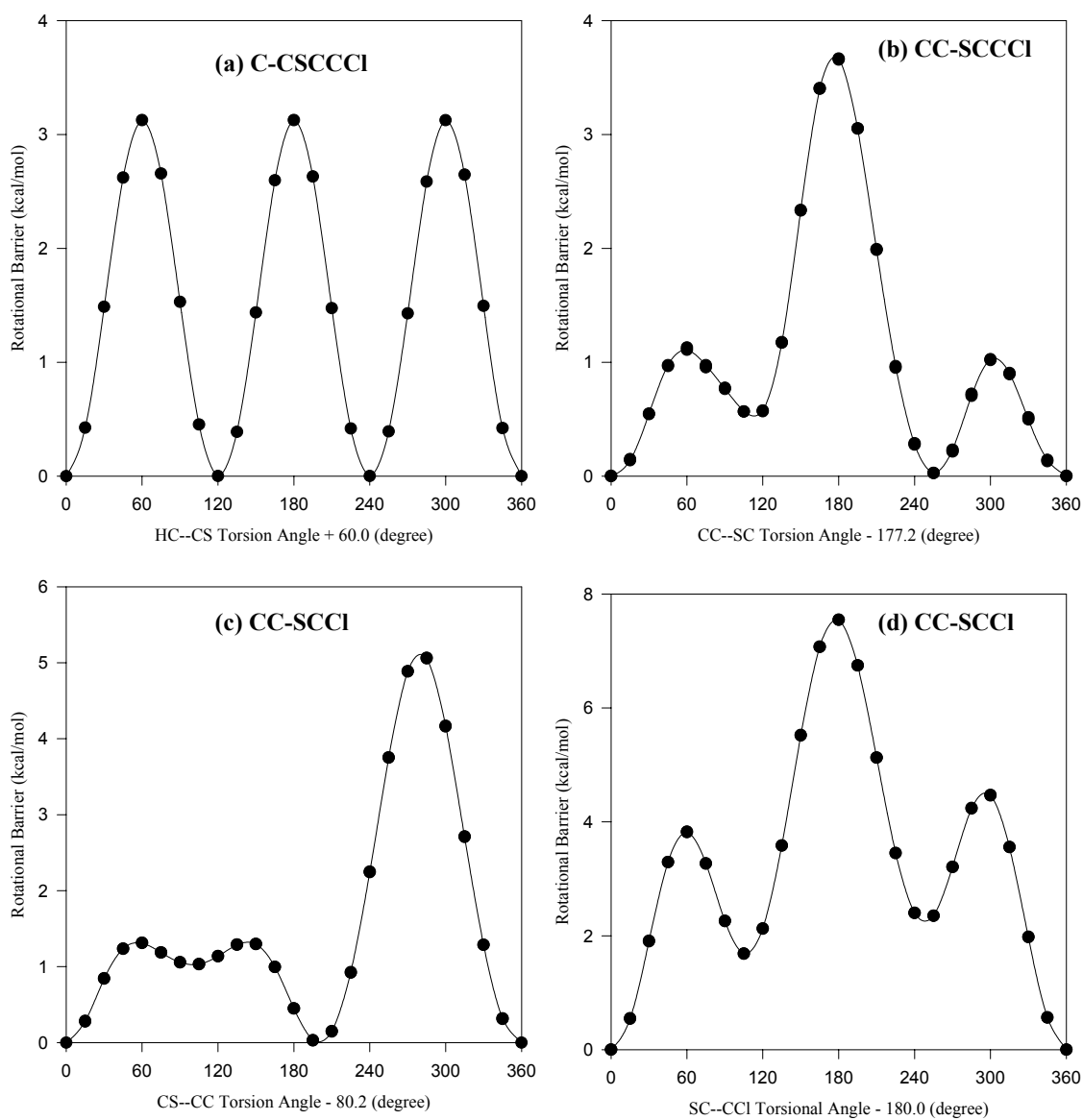


Figure 2. Potential barriers for 4 internal rotations about $\text{CH}_3\text{CH}_2\text{SCH}_2\text{CH}_2\text{Cl}$. Points are calculated values at the B3LYP/6-31G(d,p) level. Lines are Fourier expansion.

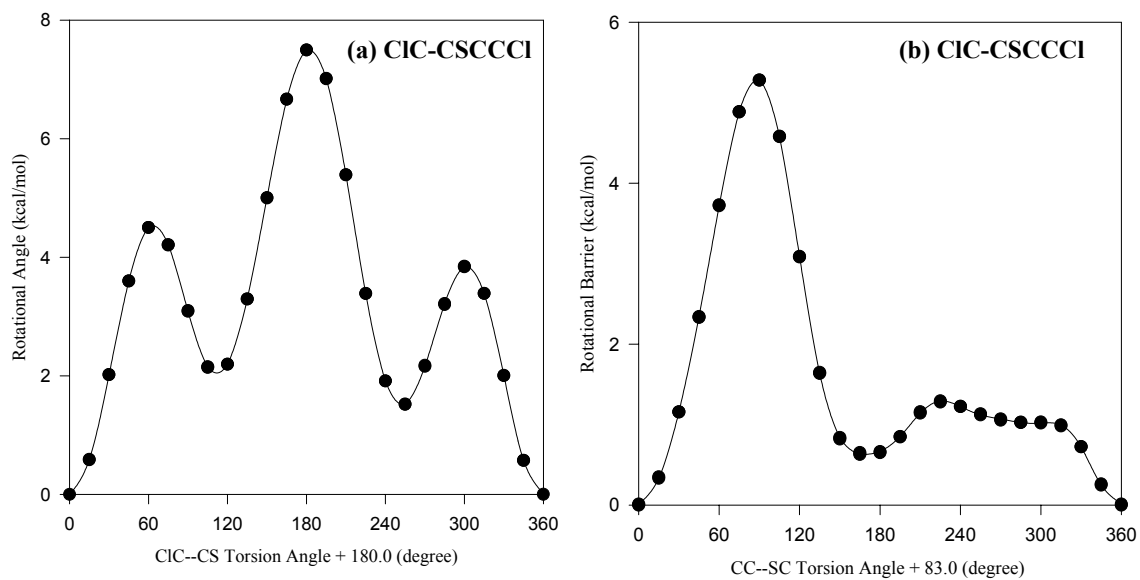


Figure 3 Potential barriers for 2 internal rotations about $\text{CH}_2\text{ClCH}_2\text{SCH}_2\text{CH}_2\text{Cl}$. Points are calculated values at the B3LYP/6-31G(d,p) level. Lines are Fourier expansions.

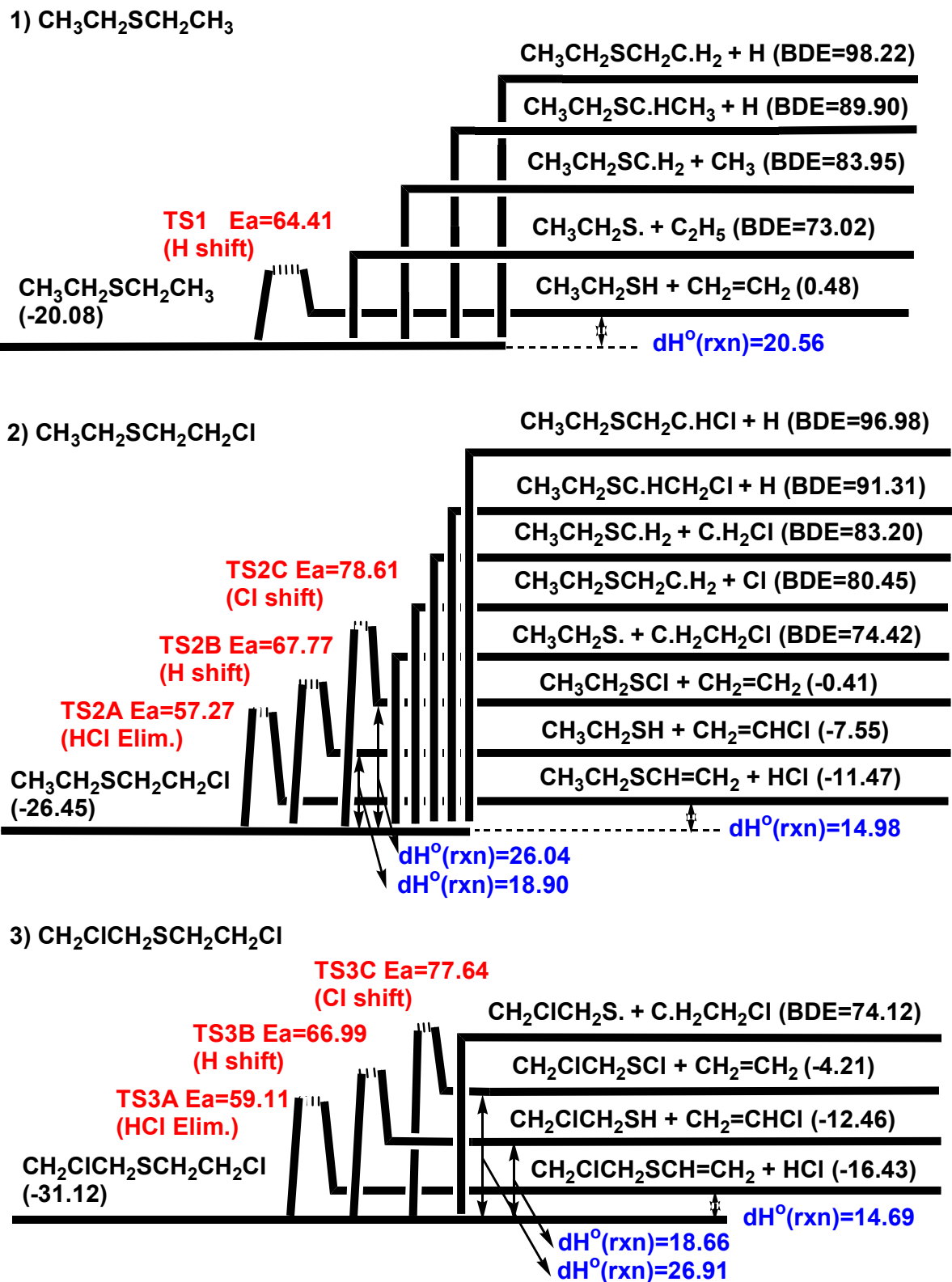
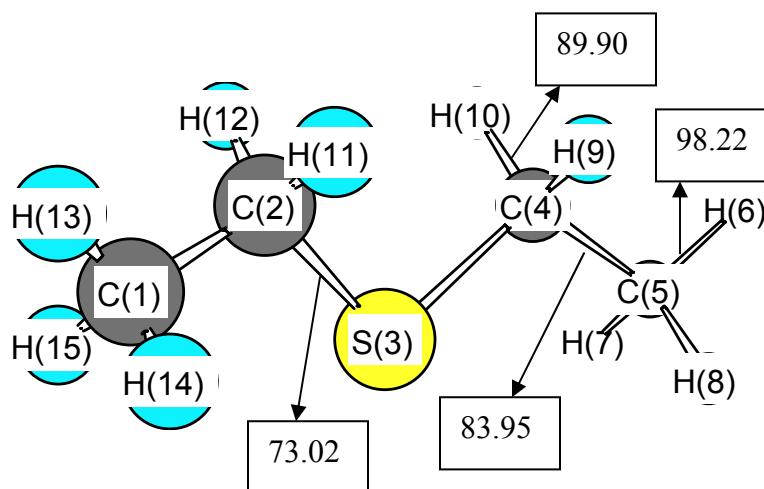


Figure 4. Potential Energy Diagram (Units: kcal/mol).

(a) $\text{CH}_3\text{CH}_2\text{SCH}_2\text{CH}_3$



(b) $\text{CH}_3\text{CH}_2\text{SCH}_2\text{CH}_2\text{Cl}$

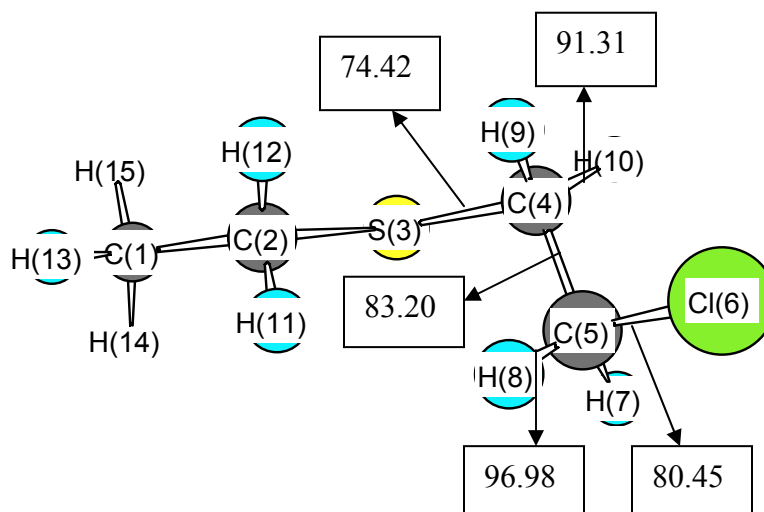


Figure 5. Bond dissociation energies^a (kcal/mol) of $\text{CH}_3\text{CH}_2\text{SCH}_2\text{CH}_3$ ^b and $\text{CH}_3\text{CH}_2\text{SCH}_2\text{CH}_2\text{Cl}$ ^c.

^a Bond energies are calculated in this work. (Table 5)

^b $\text{CH}_3\text{CH}_2\text{SCH}_2-\text{CH}_3$: $\Delta_f H^\circ_{298}$ of $[\text{C}_2\text{H}_5\text{SCH}_3] = -14.24 \pm 0.26$ (ref. 7), $[\text{CH}_3] = 34.82 \pm 0.2$ (ref. 8) and BDE of $[\text{CH}_3\text{SCH}_2-\text{H}] = 95.39$ (in this study) are used.

^c $\text{CH}_3\text{CH}_2\text{S}-\text{CH}_2\text{CH}_2\text{Cl}$: $\Delta_f H^\circ_{298}$ of $[\text{C}\cdot\text{H}_2\text{CH}_2\text{Cl}] = 23.83$ (ref. 36) is used.

^c $\text{CH}_3\text{CH}_2\text{SCH}_2-\text{CH}_2\text{Cl}$: $\Delta_f H^\circ_{298}$ of $[\text{C}\cdot\text{H}_2\text{Cl}] = 27.7 \pm 2.0$ (ref. 37) is used.

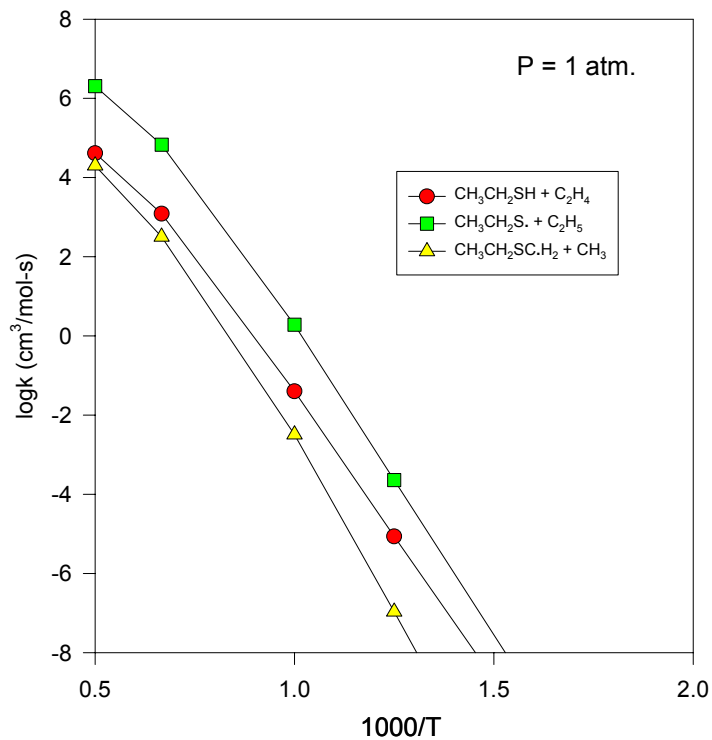


Figure 6. $\text{CH}_3\text{CH}_2\text{SCH}_2\text{CH}_3$ Dissociation constant vs. $1000/T$ at 1 atm.

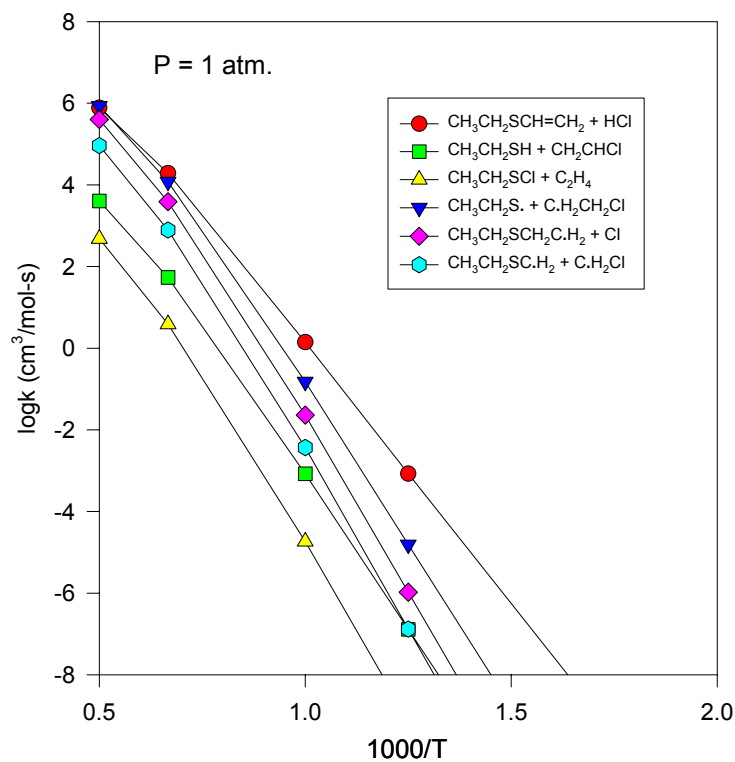


Figure 7. $\text{CH}_3\text{CH}_2\text{SCH}_2\text{CH}_2\text{Cl}$ Dissociation constant vs. $1000/T$ at 1 atm.

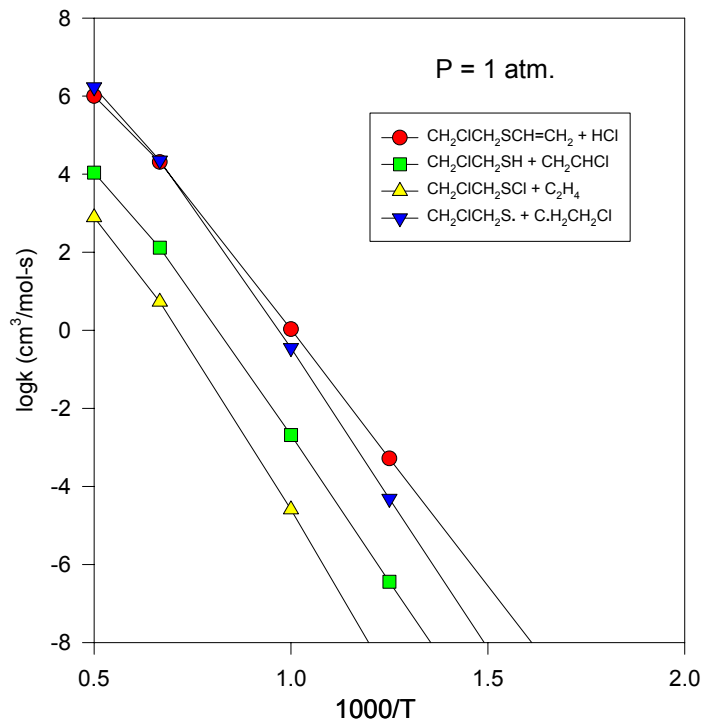


Figure 8. $\text{CH}_2\text{ClCH}_2\text{SCH}_2\text{CH}_2\text{Cl}$ Dissociation constant vs. $1000/T$ at 1 atm.

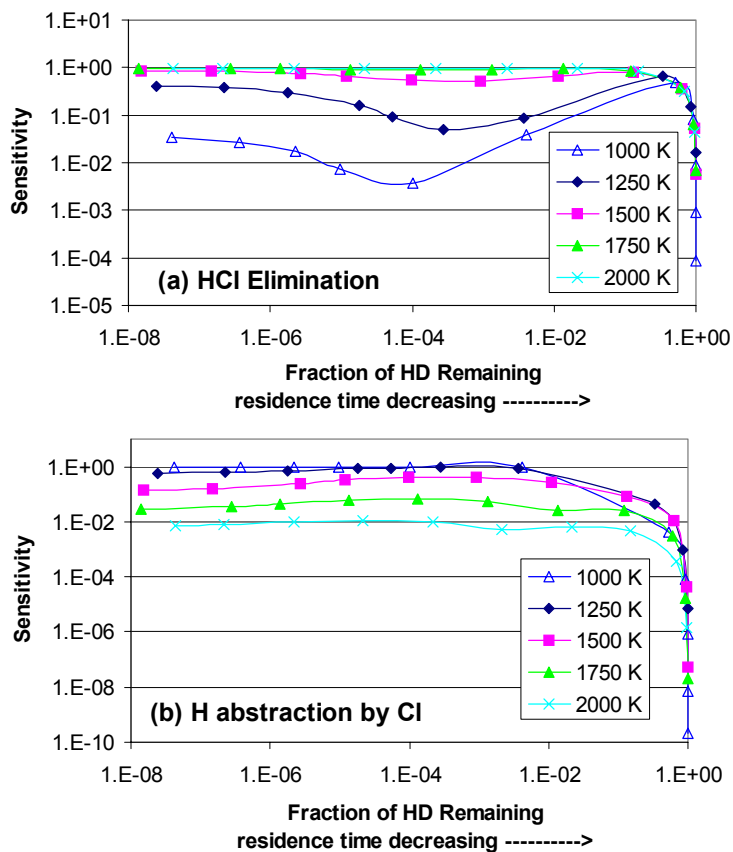


Figure 9. Calculated first order sensitivity coefficients for HD destruction in a perfectly stirred reactor for 1000 ppm of HD in air, $P = 1$ atm.

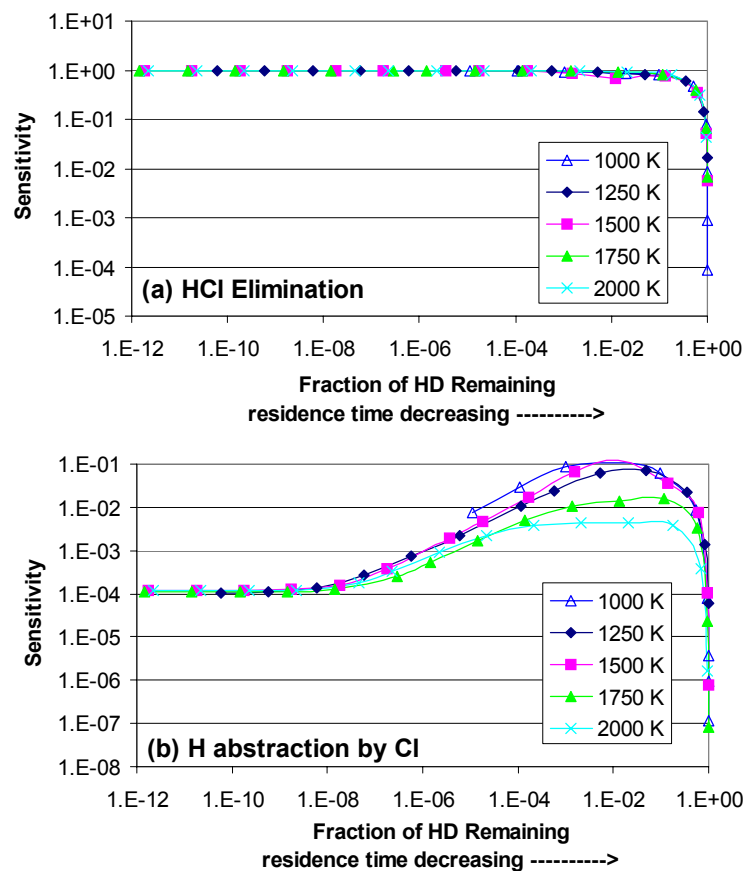


Figure 10. Calculated first order sensitivity coefficients for HD destruction in a perfectly stirred reactor for 1000 ppm of HD in lean (equivalence ratio = 0.8) CH_4 -air products with superequilibrium radicals, $P = 1$ atm.

TABLE 1: Comparison of Enthalpies of Formation at B3LYP/6-31G(d,p) with Literature Values (Units in kcal/mol).

Working Reactions	B3LYP/6-31G(d,p)		ΔH_f° ₂₉₈	
	$\Delta_{\text{rxn}} H^\circ$ ₂₉₈	$\Delta_f H^\circ$ ₂₉₈	Avg. (B3LYP) ^a	Literature
CH₃SH + CH₄ <=> CH₃CH₃ + H₂S	-1.26	-5.99	-6.22 ± 0.68	-5.47 ± 0.14[7]
CH₃SH + CH₃OH <=> CH₃CH₂OH + H₂S	-6.47	-6.44		
CH₃CH₂SH + CH₄ <=> CH₃SH + CH₃CH₃	2.52	-10.34	-10.82 ± 2.93	-11.07 ± 0.14[7]
CH₃CH₂SH + CH₃OH <=> CH₃SH + CH₃CH₂OH	-2.69	-10.79		
CH₃CH₂SH + CH₃CH₂OH <=> CH₃SH + (CH₃)₂CHOH	-3.17	-11.32		
CH₃SCH₃ + CH₄ <=> CH₃SH + CH₃CH₃	0.87	-8.69	-9.17 ± 2.93	-8.96 ± 0.12[7]
CH₃SCH₃ + CH₃OH <=> CH₃SH + CH₃CH₂OH	-4.33	-9.15		
CH₃SCH₃ + CH₃CH₂OH <=> CH₃SH + (CH₃)₂CHOH	-4.82	-9.67		
C.H₂SH + CH₃OH <=> CH₃SH + C.H₂OH	-1.13	39.85	38.72 ± 2.12	36.36 ± 2.00[14]
C.H₂SH + CH₄ <=> C.H₂CH₃ + H₂S	3.43	38.36		
C.H₂SH + CH₃OH <=> C.H₂CH₂OH + H₂S	-0.38	37.94		
CH₃S. + CH₃CH₂OH <=> CH₃SH + CH₃CH₂O.	15.97	30.83	31.39 ± 2.29	30.83 ± 1.90[18]
CH₃S. + CH₃OH <=> CH₃SH + CH₃O.	14.85	31.94		
CH₃CH₂S. + CH₃CH₂OH <=> CH₃CH₂SH + CH₃CH₂O.	15.73	25.47	25.93 ± 2.09	24.14 ± 0.96[3]
CH₃CH₂S. + CH₃OH <=> CH₃SH + CH₃CH₂O.	13.05	25.74		
CH₃CH₂S. + CH₃OH <=> CH₃CH₂SH + CH₃O.	14.62	26.57		
C.H₂CH₂SH + CH₃SH <=> CH₃CH₂SH + C.H₂SH	-3.57	34.33	35.60 ± 4.06	
C.H₂CH₂SH + CH₃CH₃ <=> CH₃CH₂SH + C.H₂CH₃	1.11	36.86		
CH₃C.HSH + CH₃SH <=> CH₃CH₂SH + C.H₂SH	2.67	28.09	29.35 ± 4.06	
CH₃C.HSH + CH₃CH₃ <=> CH₃CH₂SH + C.H₂CH₃	7.36	30.61		
C.H₂SCH₃ + CH₃OCH₃ <=> CH₃SCH₃ + CH₃OC.H₂	0.68	34.45	34.33 ± 1.23	32.27 ± 0.72[20,21]
C.H₂SCH₃ + CH₃CH₂OH <=> CH₃SCH₃ + C.H₂CH₂OH	7.30	34.21		

^a Uncertainties are sum of the standard deviation for B3LYP/6-31G(d,p) level of theory and maximum cumulative uncertainties from reference species.

TABLE 2: Enthalpies of Formation for Reference Molecules in the Isodesmic Reactions

Compounds	$\Delta_f H^\circ_{298}$ (kcal/mol)	Compounds	$\Delta_f H^\circ_{298}$ (kcal/mol)
CH ₃ SH	-5.47 ± 0.14 [7]	CH ₄	-17.89 ± 0.07^a [8]
CH ₃ CH ₃	-20.24 ± 0.10^a [9]	H ₂ S	-4.90 ± 0.19 [10]
CH ₃ CH ₂ SH	-11.07 ± 0.14 [7]	CH ₃ OH	-48.16 ± 0.07 [11]
CH ₃ CH ₂ OH	-56.17 ± 0.10^a [12]	(CH ₃) ₂ CHOH	-65.19 ± 2.2 [13]
CH ₃ SCH ₃	-8.96 ± 0.12 [7]	C.H ₂ SH	36.36 ± 2.0 [14]
C.H ₂ OH	-3.97 ± 0.22 [15]	C.H ₂ CH ₃	28.80 ± 0.50 [16]
C.H ₂ CH ₂ OH	-5.70 ± 0.85 [17]	CH ₃ S.	30.83 ± 1.90 [18]
CH ₃ CH ₂ O.	-3.90 ± 1.27 [15]	CH ₃ O.	4.10 ± 1.0 [19]
CH ₃ CH ₂ S.	24.14 ± 0.96 [3]	C.H ₂ SCH ₃	32.27 ± 0.72 [20,21]
CH ₃ CH ₂ SCH ₂ CH ₃	-20.08 ± 0.24 [7]	CH ₃ CH ₂ Cl	-26.80 ± 0.26^a [8]
CH ₂ ClCH ₂ Cl	-30.33 ± 0.67 [11]	CH ₃ OCH ₃	-43.99 ± 0.12 [11]
CH ₃ OC.H ₂	0.1 [22]	CH ₃ C.HOH	-13.34 ± 0.84 [15]

^a The uncertainties are evaluated from reference [11].

TABLE 3: Reaction Enthalpies and Enthalpies of Formation in the Isodesmic Reactions
(Units in kcal/mol).

Working Reactions	$\Delta_{\text{rxn}}H_{298}^{\circ}$		$\Delta_f H_{298}^{\circ}$	
	B3LYP	KMLYP	B3LYP	KMLYP
C.H₂CH₂SH + CH₃SH <=> CH₃CH₂SH + C.H₂SH	-3.57	-4.45	34.33	35.21
CH₃C.HSH + CH₃SH <=> CH₃CH₂SH + C.H₂SH	2.67	1.82	28.09	28.94
CH₃CH₂SCH₂C.H₂ + CH₃CH₂SH <=> CH₃CH₂SCH₂CH₃ + C.H₂CH₂SH	-0.72	-0.49	26.04	26.69
CH₃CH₂SC.HCH₃ + CH₃CH₂SH <=> CH₃CH₂SCH₂CH₃ + CH₃C.HSH	1.36	1.21	17.72	18.72
CH₃CH₂SCH₂CH₂Cl + CH₃CH₃ <=> CH₃CH₂SCH₂CH₃ + CH₃CH₂Cl	-0.19	-0.23	-26.45	-26.41
CH₂ClCH₂SCH₂CH₂Cl + CH₃CH₃ <=> CH₃CH₂SCH₂CH₃ + CH₂ClCH₂Cl	0.95	1.18	-31.12	-31.35
CH₃CH₂SCH₂C.HCl + CH₃CH₂OH <=> CH₃CH₂SCH₂CH₂Cl + C.H₂CH₂OH	5.71	4.70	18.32	19.36
CH₃CH₂SCH₂C.HCl + CH₃OCH₃ <=> CH₃CH₂SCH₂CH₂Cl + CH₃OC.H₂	-0.91	-1.69	18.55	19.38
Average ^a for CH₃CH₂SCH₂C.HCl				18.43 ± 1.71 (B3LYP)
				19.37 ± 1.56 (KMLYP)
CH₃CH₂SC.HCH₂Cl + CH₃CH₂OH <=> CH₃CH₂SCH₂CH₂Cl + CH₃C.HOH	2.80	0.99	13.58	15.43
CH₃CH₂SC.HCH₂Cl + CH₃OCH₃ <=> CH₃CH₂SCH₂CH₂Cl + CH₃OC.H₂	5.70	3.06	11.95	14.62
Average ^a for CH₃CH₂SC.HCH₂Cl^b				12.76 ± 2.69 (B3LYP)
				15.03 ± 2.11 (KMLYP)

^a Uncertainties are sum of the standard deviation for each calculation level of theory and maximum cumulative uncertainties from reference species.

^b The values between B3LYP and KMLYP have 2.3 kcal/mol difference, so further calculations were performed. 12.71 ± 2.18 (B3LYP/6-311G(d,p)) and 12.85 ± 1.65 (CBSQ), so B3LYP value is recommended.

TABLE 4: Comparison of Activation Energies (Units in kcal/mol).

	B3LYP/6- 31G(d,p)	KMLYP/6- 311G(d,p)	CBS-Q	CBS- QB3
<H Shift>				
TS1	61.51	73.42	65.46	64.41
TS2B	65.62	78.08	68.62	67.77
TS3B	64.15	76.93	66.81	66.99
<Cl Shift>				
TS2C	73.54	95.29	80.89	78.61
TS3C	73.31	94.80	79.57	77.64
<HCl Elimination>				
TS2A	52.25	59.04	58.06	57.27
TS3A	54.27	61.42	60.08	59.11

TABLE 5: Ideal Gas Phase Thermodynamic Properties Obtained by B3LYP/6-31G(d,p) Calculation^a

Species (s, e, OI) ^g		$\Delta_f H_{298}^{\circ}$ ^b	S_{298}° ^c	Cp_{300}° ^c	Cp_{400}	Cp_{500}	Cp_{600}	Cp_{800}	Cp_{1000}	Cp_{1500}
REACTANTS										
CH₃CH₂SCH₂CH₃	TVR ^d		66.19	19.36	25.96	32.18	37.59	46.23	52.73	62.98
(C-CSCC)	I. R. ^f		4.40	2.11	2.12	2.02	1.88	1.63	1.46	1.23
(CC-SCC)	I. R.		7.49	1.72	1.57	1.48	1.41	1.31	1.24	1.13
(CCS-CC)	I. R.		7.49	1.72	1.57	1.48	1.41	1.31	1.24	1.13
(CCSC-C)	I. R.		4.40	2.11	2.12	2.02	1.88	1.63	1.46	1.23
(18,0,1)	Total	-20.08	89.97	27.02	33.34	39.18	44.17	52.11	58.13	67.70
CH₃CH₂SCH₂CH₂Cl	TVR ^d		75.47	22.00	28.87	35.10	40.38	48.62	54.70	64.16
(C-CSCCCI)	I. R. ^f		4.40	2.11	2.12	2.02	1.88	1.63	1.46	1.23
(CC-SCCCI)	I. R.		7.49	1.72	1.57	1.48	1.41	1.31	1.24	1.13
(CCS-CCCI)	I. R.		7.44	2.27	1.92	1.73	1.61	1.47	1.37	1.23
(CCSC-CCI)	I. R.		5.73	3.67	3.77	3.49	3.12	2.51	2.11	1.59
(3,0,1)	Total	-26.45	100.53	31.77	38.25	43.82	48.40	55.54	60.88	69.34
CH₂ClCH₂SCH₂CH₂Cl	TVR ^d		82.45	24.60	31.74	38.00	43.16	51.01	56.66	65.34
(ClC-CSCCCI)	I. R. ^f		5.95	3.75	3.71	3.38	3.01	2.43	2.06	1.57
(ClCC-SCCCI)	I. R.		7.86	2.14	1.77	1.61	1.52	1.42	1.35	1.22
(ClCCS-CCCI)	I. R.		7.86	2.14	1.77	1.61	1.52	1.42	1.35	1.22
(ClCCSC-CCI)	I. R.		5.95	3.75	3.71	3.38	3.01	2.43	2.06	1.57
(1,0,1)	Total	-31.12	110.07	36.38	42.70	47.98	52.22	58.71	63.48	70.92
TRANSITION STATES										
TS1	TVR ^d		74.88	24.34	31.13	37.25	42.45	50.59	56.62	66.06
(C-CSCC)	I. R. ^f		4.40	2.11	2.12	2.02	1.88	1.63	1.46	1.23
(CC-SCC)	I. R.		7.49	1.72	1.57	1.48	1.41	1.31	1.24	1.13
(3,0,1)	Total	44.33	86.77	28.17	34.82	40.75	45.74	53.53	59.32	68.42
TS2A	TVR ^d		78.71	25.12	31.93	37.96	43.01	50.79	56.45	65.20
(C-CSCCCI)	I. R. ^f		4.40	2.11	2.12	2.02	1.88	1.63	1.46	1.23
(CC-SCCCI)	I. R.		7.49	1.72	1.57	1.48	1.41	1.31	1.24	1.13
(CCS-CCCI)	I. R.		7.44	2.27	1.92	1.73	1.61	1.47	1.37	1.23
(3,0,1)	Total	30.82	98.04	31.22	37.54	43.19	47.91	55.20	60.52	68.79
TS2B	TVR ^d		81.67	27.31	34.28	40.34	45.37	53.08	58.68	67.33
(C-CSCCCI)	I. R. ^f		4.40	2.11	2.12	2.02	1.88	1.63	1.46	1.23
(CC-SCCCI)	I. R.		7.49	1.72	1.57	1.48	1.41	1.31	1.24	1.13
(3,0,1)	Total	41.32	93.56	31.14	37.97	43.84	48.66	56.02	61.38	69.69
TS2C	TVR ^d		85.11	27.96	34.32	39.94	44.67	52.09	57.66	66.55
(C-CSCCCI)	I. R. ^f		4.40	2.11	2.12	2.02	1.88	1.63	1.46	1.23
(CC-SCCCI)	I. R.		7.49	1.72	1.57	1.48	1.41	1.31	1.24	1.13
(3,0,1)	Total	52.16	97.00	31.79	38.01	43.44	47.96	55.03	60.36	68.91
TS3A	TVR ^d		87.38	27.74	34.77	40.82	45.77	53.16	58.42	66.40
(ClC-CSCCCI)	I. R. ^f		5.95	3.75	3.71	3.38	3.01	2.43	2.06	1.57
(ClCC-SCCCI)	I. R.		7.86	2.14	1.77	1.61	1.52	1.42	1.35	1.22
(ClCCS-CCCI)	I. R.		7.86	2.14	1.77	1.61	1.52	1.42	1.35	1.22
(1,0,1)	Total	27.99	109.05	35.77	42.02	47.42	51.82	58.43	63.18	70.41
TS3B	TVR ^d		90.45	29.93	37.10	43.17	48.09	55.42	60.61	68.49
(ClC-CSCCCI)	I. R. ^f		5.95	3.75	3.71	3.38	3.01	2.43	2.06	1.57
(ClCC-SCCCI)	I. R.		7.86	2.14	1.77	1.61	1.52	1.42	1.35	1.22
(1,0,1)	Total	35.87	104.26	35.82	42.58	48.16	52.62	59.27	64.02	71.28
TS3C	TVR ^d		92.58	30.43	37.08	42.74	47.38	54.44	59.61	67.74
(ClC-CSCCCI)	I. R. ^f		5.95	3.75	3.71	3.38	3.01	2.43	2.06	1.57

TABLE 5: (Continued) Ideal Gas Phase Thermodynamic Properties Obtained by B3LYP/6-31G(d,p) Calculation^a

(CICC-SCCCL)	I. R.		7.86	2.14	1.77	1.61	1.52	1.42	1.35	1.22
(1,0,1)	Total	46.52	106.39	36.32	42.56	47.73	51.91	58.29	63.02	70.53
PRODUCTS										
CH₃CH₂SCH₂C.H₂	TVR ^d		71.66	20.15	26.31	31.88	36.61	44.09	49.72	58.66
(C-CSCC)	I. R. ^f		4.40	2.11	2.12	2.02	1.88	1.63	1.46	1.23
(CC-SCC)	I. R.		7.49	1.72	1.57	1.48	1.41	1.31	1.24	1.13
(CCS-CC)	I. R.		7.49	1.72	1.57	1.48	1.41	1.31	1.24	1.13
(CCSC-C)	I. R.		4.40	2.11	2.12	2.02	1.88	1.63	1.46	1.23
(3,1/2,1)	Total	26.04	95.44	27.81	33.69	38.88	43.19	49.97	55.12	63.38
CH₃CH₂SC.HCH₃	TVR ^d		69.19	19.66	25.69	31.27	36.08	43.74	49.50	58.60
(C-CSCC)	I. R. ^f		4.40	2.11	2.12	2.02	1.88	1.63	1.46	1.23
(CC-SCC)	I. R.		7.49	1.72	1.57	1.48	1.41	1.31	1.24	1.13
(CCS-CC)	I. R.		7.49	1.72	1.57	1.48	1.41	1.31	1.24	1.13
(CCSC-C)	I. R.		4.40	2.11	2.12	2.02	1.88	1.63	1.46	1.23
(9,1/2,1)	Total	17.72	92.97	27.32	33.07	38.27	42.66	49.62	54.90	63.32
CH₃CH₂SCH₂C.HCl	TVR ^d		77.13	22.39	28.71	34.29	38.96	46.20	51.53	59.83
(C-CSCCCL)	I. R. ^f		4.40	2.11	2.12	2.02	1.88	1.63	1.46	1.23
(CC-SCCCL)	I. R.		7.49	1.72	1.57	1.48	1.41	1.31	1.24	1.13
(CCS-CCCL)	I. R.		7.44	2.27	1.92	1.73	1.61	1.47	1.37	1.23
(CCSC-CCl)	I. R.		5.73	3.67	3.77	3.49	3.12	2.51	2.11	1.59
(3,1/2,1)	Total	18.43	102.19	32.16	38.09	43.01	46.98	53.12	57.71	65.01
CH₃CH₂SC.HCH₂Cl	TVR ^d		76.51	22.33	28.62	34.18	38.84	46.07	51.39	59.71
(C-CSCCCL)	I. R. ^f		4.40	2.11	2.12	2.02	1.88	1.63	1.46	1.23
(CC-SCCCL)	I. R.		7.49	1.72	1.57	1.48	1.41	1.31	1.24	1.13
(CCS-CCCL)	I. R.		7.44	2.27	1.92	1.73	1.61	1.47	1.37	1.23
(CCSC-CCl)	I. R.		5.73	3.67	3.77	3.49	3.12	2.51	2.11	1.59
(3,1/2,1)	Total	12.76	101.57	32.10	38.00	42.90	46.86	52.99	57.57	64.89
CH₃CH₂SH	TVR ^d		62.12	13.43	17.03	20.40	23.34	28.11	31.74	37.51
(C-CSH)	I. R. ^f		4.27	2.10	2.16	2.09	1.96	1.71	1.53	1.27
(CC-SH)	I. R.		4.57	1.94	1.64	1.44	1.32	1.19	1.12	1.05
(3,0,1)	Total	-10.82	70.96	17.47	20.83	23.93	26.62	31.01	34.39	39.83
CH₃CH₂S.	TVR ^d		63.58	13.65	16.85	19.82	22.39	26.53	29.67	34.64
(C-CS)	I. R. ^f		4.50	2.09	2.06	1.94	1.79	1.55	1.40	1.20
(3,1/2,1)	Total	25.93	68.08	15.74	18.91	21.76	24.18	28.08	31.07	35.84
CH₃CH₂SCl	TVR ^d		68.19	15.91	19.55	22.82	25.61	30.00	33.28	38.42
(C-CSCl)	I. R. ^f		4.40	2.11	2.13	2.03	1.89	1.64	1.46	1.23
(CC-SCl)	I. R.		6.69	2.21	2.07	1.92	1.78	1.56	1.42	1.22
(3,0,1)	Total	-12.95	79.28	20.23	23.75	26.77	29.28	33.20	36.16	40.87
CH₃CH₂SCHCH₂	TVR ^d		69.15	19.38	25.37	30.70	35.20	42.23	47.47	55.73
(C-CSC=C)	I. R. ^f		4.48	2.14	2.11	1.97	1.82	1.57	1.40	1.20
(CC-SC=C)	I. R.		6.85	2.13	1.90	1.75	1.65	1.49	1.38	1.22
(CCS-C=C)	I. R.		6.17	2.24	2.09	1.93	1.78	1.55	1.40	1.20
(3,0,1)	Total	10.59	86.65	25.89	31.47	36.35	40.45	46.84	51.65	59.35
CH₂ClCH₂SCl	TVR ^d		76.25	18.46	22.34	25.63	28.31	32.34	35.21	39.60
(ClC-CSCl)	I. R. ^f		5.72	3.26	3.38	3.30	3.10	2.65	2.27	1.72
(CICC-SCl)	I. R.		6.89	2.39	2.43	2.31	2.14	1.83	1.61	1.32
(1,0,1)	Total	-16.75	88.86	24.11	28.15	31.24	33.55	36.82	39.09	42.64

a : Thermodynamic properties are referred to a standard state of an ideal gas of pure enantiomer at 1 atm.

b : Units in kcal/mol c : Units in cal/mol-K

d : Sum of contributions from translations, vibrations, and external rotations.

f : I. R. represents contribution from internal rotation

g : Symmetry number, optical isomer and electronic spin are taken into account, -Rln(s), Rln2, Rln2, respectively.

s = number of symmetry, e = electronic spin, OI = number of optical isomer

TABLE 6: Bond energies at 298K (kcal/mol).

Reaction series	Bond energies		
	B3LYP ^a	KMLYP ^b	Literature ^c
$\text{CH}_3\text{SH} \Rightarrow \text{CH}_3\text{S} \cdot + \text{H} \cdot$	88.96 ± 2.43	-	$88.40 \pm 2.04[7,18]$
$\text{CH}_3\text{SH} \Rightarrow \text{C} \cdot\text{H}_2\text{SH} + \text{H} \cdot$	96.29 ± 2.26	-	$93.93 \pm 2.14[7,14]$
$\text{CH}_3\text{CH}_2\text{SH} \Rightarrow \text{CH}_3\text{CH}_2\text{S} \cdot + \text{H} \cdot$	89.10 ± 2.23	-	$87.31 \pm 1.10[7,3]$
$\text{CH}_3\text{CH}_2\text{SH} \Rightarrow \text{C} \cdot\text{H}_2\text{CH}_2\text{SH} + \text{H} \cdot$	98.77 ± 4.20	98.38 ± 4.20	n/a
$\text{CH}_3\text{CH}_2\text{SH} \Rightarrow \text{CH}_3\text{C} \cdot\text{HSH} + \text{H} \cdot$	92.52 ± 4.20	92.11 ± 4.20	n/a
$\text{CH}_3\text{SCH}_3 \Rightarrow \text{C} \cdot\text{H}_2\text{SCH}_3 + \text{H} \cdot$	95.39 ± 1.35	-	$93.33 \pm 0.84[7,20,21]$
$\text{CH}_3\text{CH}_2\text{SCH}_2\text{CH}_3 \Rightarrow \text{CH}_3\text{CH}_2\text{SCH}_2\text{C} \cdot\text{H}_2 + \text{H} \cdot$	98.22 ± 2.90	98.87 ± 2.90	n/a
$\text{CH}_3\text{CH}_2\text{SCH}_2\text{CH}_3 \Rightarrow \text{CH}_3\text{CH}_2\text{SC} \cdot\text{HCH}_3 + \text{H} \cdot$	89.90 ± 2.90	90.90 ± 2.90	n/a
$\text{CH}_3\text{CH}_2\text{SCH}_2\text{CH}_2\text{Cl} \Rightarrow \text{CH}_3\text{CH}_2\text{SCH}_2\text{C} \cdot\text{HCl} + \text{H} \cdot$	96.98 ± 1.71	97.88 ± 1.56	n/a
$\text{CH}_3\text{CH}_2\text{SCH}_2\text{CH}_2\text{Cl} \Rightarrow \text{CH}_3\text{CH}_2\text{SC} \cdot\text{HCH}_2\text{Cl} + \text{H} \cdot$	91.31 ± 2.69	93.53 ± 2.11	n/a

^a Uncertainties are sum of the standard deviation for B3LYP/6-31G(d,p) level of theory and maximum cumulative uncertainties from reference species.

^b Uncertainties are sum of the standard deviation for KMLYP/6-311G(d,p) level of theory and maximum cumulative uncertainties from reference species.

^c Uncertainties are sum of maximum cumulative uncertainties from reference species.